Near-wall fluid mechanics of a pulsatile flow through a compliant tube

Guilherme M. Bessa, Jake Hadfield and David S. Nobes*
Dept. of Mechanical Engineering, University of Alberta, Canada
* Correspondent author: dnobes@ualberta.ca

Keywords: Compliance, Fluid-solid interaction, PIV investigation, Biomedical flows

ABSTRACT

The demand for heart transplantation far exceeds the supply. This shortage is mainly due to the high percentage of discarded hearts and the narrow time window of only six hours that the current standard preservation method, static cold storage (SCS), allows for completing the entire procedure from donor to recipient patient. An alternative method called ex-vivo heart perfusion (EVHP) maintains a human donor heart beating outside the body for the time preceding transplantation surgery. By keeping the donor heart beating in a quasi-physiological mode of operation and assessing its functions, the organ's health can be monitored so that, ultimately, the transplant time window can be extended to increase the geographic availability of donors. In order to improve and optimize the EVHP system, fundamental understanding of the system physics is needed. To achieve this, the present work aims to investigate the relationship between pulsatile flow and compliance, evaluating the near wall region of a compliant tube with a particular focus on the formation of the viscous boundary layer. Thus, an experimental setup was designed to replicate the flow loop of the EVHP system and an optically transparent compliant tube that mimics the functioning of the body's largest and most compliant artery, the aorta, was custom-made to allow optical access to the flow field matching the refractive index of the working fluid. A pulsatile waveform is generated using a computer-controlled mechanical diaphragm pump, also equipped with a tri-leaf exit valve to simulate the physiological working condition of the heart. In the present work, the flow field is assessed by first performing stereo particle image velocimetry (PIV) on the bulk flow to investigate the large-scale phenomena within a compliant tube and the results of these experiments will be further used as a guide to interrogate smaller near-wall regions of interest in the flow. The preliminary results show, in addition to the general characteristics of a pulsatile flow through a compliant tube, a potential complex fluid-structure relationship between the pulsatile flow and the moving wall of the tube has been observed. The presentation of this work will discuss the experimental setup and review the preliminary results presented here in addition to others findings that are still being analyzed, data processing is underway to do so.

1. Introduction

The motivation for this study comes from investigations into an Ex-Vivo Heart Perfusion (EVHP) system that is under development by researchers in the Department of Surgery at the University of Alberta (White et al., 2020). Such a system is primarily intended to keep donor hearts in working mode as a preservation technique for heart transplant surgery. By keeping the heart beating and pumping fluid in a quasi-physiological mode of functioning, it becomes feasible to monitor the organ's performance to ensure that the patient's transplant procedure is completed with greater chances of success (White et al., 2020). In addition, this new technique may eventually allow damaged hearts to be recovered and used for transplantation, whereas with classical means of preservation such organs would be discarded for safety reasons. Thus, this shows promise in improving the pool of available donor hearts (White et al., 2020). In a previous study it was shown that the addition of a compliant tubing section in the flow loop of the EVHP system could adjust the flow-pressure regime of the pulsatile flow to be closer to the physiological regime (Cameron et al., 2020). This had the added effect of reducing the heart workload (Cameron et al., 2020). The current study aims to further investigate the relationship between pulsatile flow and compliance, focusing mainly on the near-wall fluid mechanics of pulsatile flow through a compliant tube. To do so, a flow loop powered by a computer-controlled mechanical diaphragm pump equipped with a three-leaf outlet valve is used to simulate the physiological working condition of the heart. The experimental setup is also designed with a custom image acquisition section to allow flow measurements with particle image velocimetry (PIV).

Past studies on this subject addressed it mainly through in vitro investigations with complex aortic models aimed at considering a realistic physiological geometry (Geoghegan et al., 2012). Although useful for understanding entirely physiological flows, the inclusion of these actual vascular features at such a level of complexity in the EVHP system is undesirable. Therefore, understanding the pulsatile flow as it exits an analogue heart pump in a simplified configuration, such as a flexible straight tube, is of greater relevance in this case. The theory of pulsatile flow is well-founded (Womersley, 1955; Ku, 1997; Wood, 1999; Langlois & Deville, 1964). In a remarkable study, Womersley (1955) proposed a method to characterize and quantify a pulsatile flow in a straight and rigid circular tube. The resultant dimensionless quantity, the Womersley number (α), establishes a relationship between the unsteady and viscous effects of a pulsatile flow. Subsequently, efforts were made to better understand the turbulent phenomena intrinsic to pulsatile flows through techniques such as hot-wire anemometry (Hino, Sawamoto & Takasu, 1976), dye-based flow visualization (Das & Arakeri, 1998) and laser Doppler velocimetry (Lodahl, Sumer & Fredsøe, 1998). The main drawback of these studies is that they struggle to identify coherent flow structures, being at best capable of defining length scales.

More recently, this problem has been addressed through 2D PIV, with more success. Brindise & Vlachos (2018) investigated the effect of pulsatile waveform input on the initiation and development mechanisms of the laminar-turbulent transition, which, in fact, is more similar to the flow regime under investigation in the present work. However, assuming that turbulence is isotropic in the direction orthogonal to the measurement plane, as is often necessary to estimate complete turbulent statistics using 2D PIV, can lead to a misunderstanding of the underlying physical phenomena.

The main objective of this study is to achieve a better understanding of how tube compliance influences flow development in a pulsatile regime. A particular focus will be on the forming viscous boundary layer, first by performing 2D PIV on the bulk flow and then using a stereo PIV configuration at key locations in the region close to the compliant tube wall. This will not only allow for a spatial assessment of large-scale flow structures, but also to extract turbulent statistics from three-component (2D3C) PIV measurements at sites of interest. The novelty and challenge in this work lies in obtaining the full three components of velocity in the fluid flow in the near-wall region of the moving boundary of the compliant tube. The inherent characteristics of a pulsatile flow interacting with the moving walls of a flexible tube make the flow field of interest a unique region to investigate. Accordingly, achieving a better understanding of this flow field is not only interesting from a fluid mechanics perspective, but will ultimately be used to improve the design of the EVHP system discussed here.

2. Experimental Design

The experiments carried out feature a custom-designed pumping system that works in a quasi-physiological mode according to the function of the human heart. A schematic representation of the experimental setup is shown in Figure 1. A silicone tri-leaf valve is used at the pump's exit to ensure mono-directional flow, and the flow loop resembles that of the EVHP system. A custom image acquisition section allows flow visualization in both the compliant section of the flow loop and the non-compliant sections upstream and downstream of the compliant tube. This imaging section is comprised of three chambers that allow sufficient optical access for PIV measurements in either a planar (2D2C) or stereo (2D3C) configuration.

A pulsatile waveform is generated using a computer-controlled mechanical diaphragm pump (PX05, ARO®) to simulate the physiological working condition of the heart. The diaphragm pump is driven by a CNC stepper motor (CPM-SCSK-3441S-ELSA, Teknic Inc.), which in turn is controlled by a function generator. Thus, the flow generated by the pump can be precisely regulated to match the physiological range of heart stroke volume and rate. The flow curve produced by the pump was designed to temporally match the shape of a right ventricle volume curve found in the literature (Konings & Jansen, 2017) at any desired pump stroke volume. The experimental flow loop was also equipped with an afterload centrifugal pump (RFC 20-970, Jostra AB) to control the back pressure of the system. However, the preliminary measurement case discussed here did not have any additional back pressure applied using this device. Instead, a restriction was included in the tubing downstream of the imaging sections, producing a more flow-dependent pressure drop in the system than in the experimental configuration discussed in the abstract.

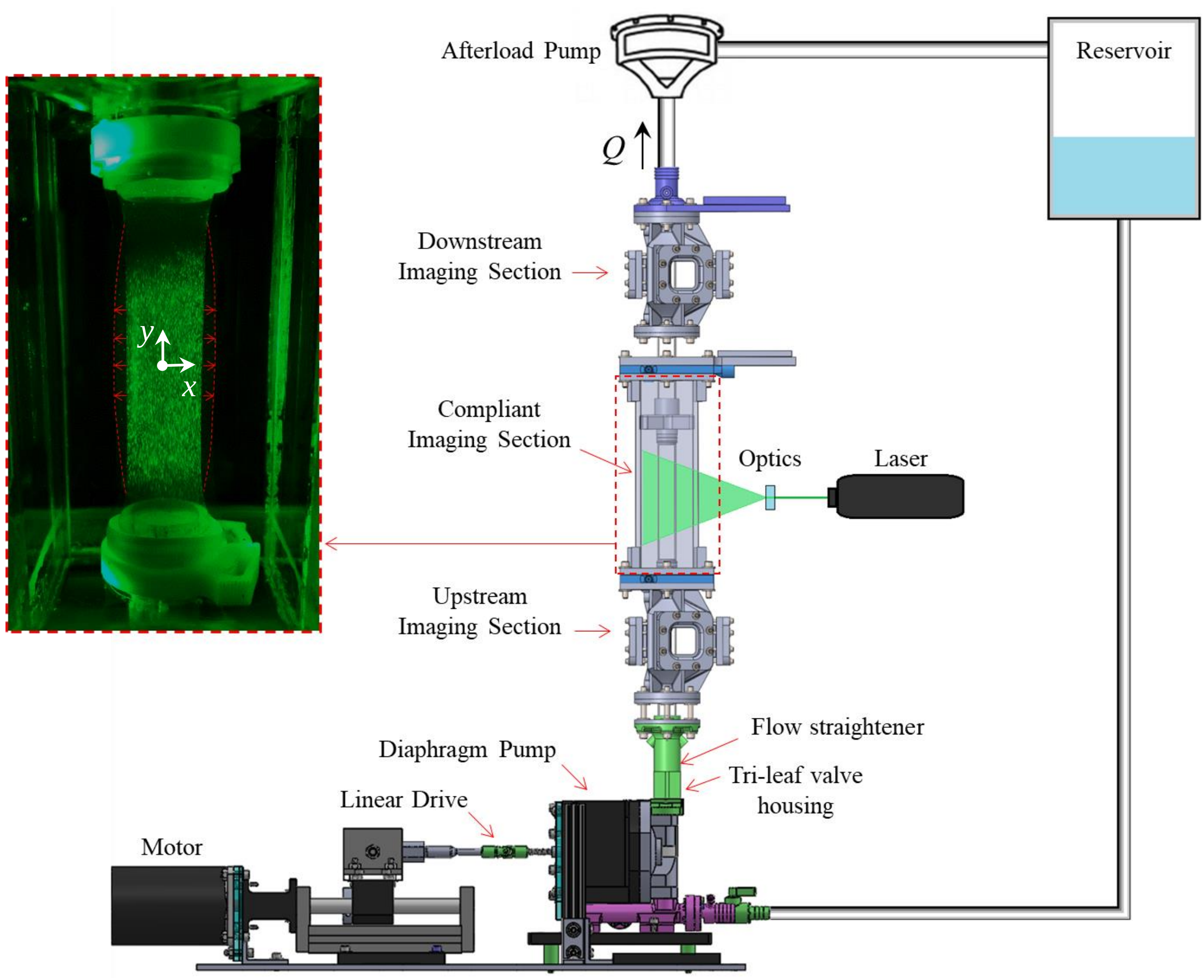

Fig. 1 Schematic of the experimental setup. On the left side, a photo figuratively shows the expected wall boundary motion.

The standard inlet and outlet of the diaphragm pump contain check valves to ensure unidirectional flow. The original outlet valve was replaced with a custom-molded tri-leaf valve in order to mimic the action of the human aortic valve. To better illustrate, an example of such a custom valve can be seen in Figure 2. The valve casting process involves first manufacturing the molds with an SLA 3D printer (Form 3, FormLabs), followed by molding with silicone (Dragon

Skin 10 Slow, Smooth-On, Inc.). Immediately after the valve, a honeycomb flow straightener coupled with a pressure drop mesh are included to reduce any flow asymmetry produced by the valve geometry.

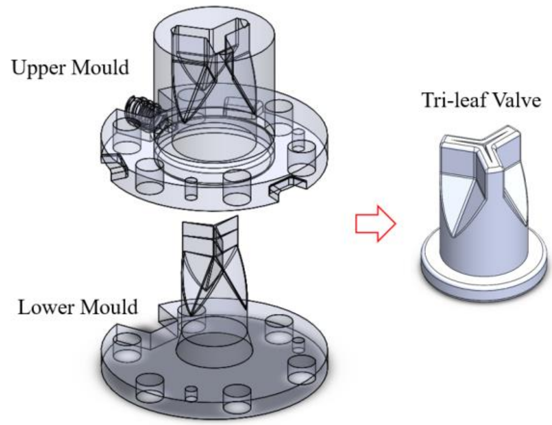

Fig. 2 3D CAD models of custom joker-type tri-leaf valve and mould.

The compliant tube was made by an in-house molding process similar to the tri-leaf valve previously described. However, in this case, the mold was developed with two concentric acrylic tubes held in place by a pair of FDM-printed end caps (Ultimaker 2/2+, Ultimaker) that allowed the injection of silicone. The silicone (Solaris, Smooth-On, Inc.) was chosen as it is optically transparent, allowing optical access to the flow field, while having more compliance (Shore A hardness of 15) than more commonly used silicones (i.e. Sylgard 184, Dow Corning Inc. Shore A hardness of 50). The finished silicone tube had a 19 mm inner diameter was 3 mm thick and 120 mm long, as seen in Figure 3 alongside to its mold.

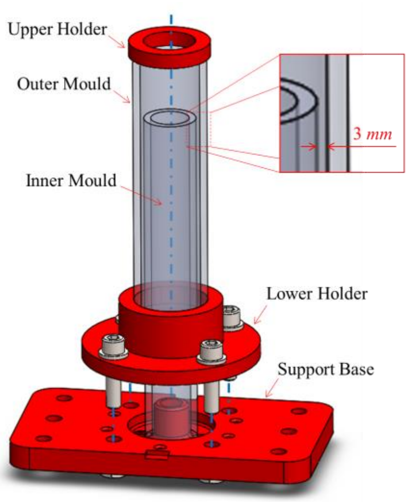

(a)

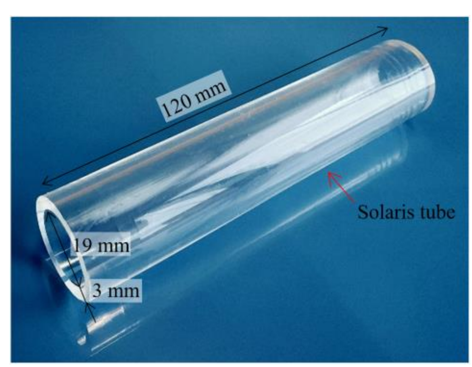

(b)

Fig. 3 (a) 3D CAD model of the tube mould; (b) photo of the completed Solaris silicone tube.

To avoid optical distortion of the acquired images, a working fluid solution was prepared with water and 57 w/w% potassium thiocyanate (KSCN) to ensure that its refractive index was compatible with that of the compliant tube material, n = 1.4072. The refractive index matched (RIM) fluid was used for both the working fluid inside the tube and its surroundings inside the visualization chamber. Figure 4 shows the effectiveness of refractive index matching. Here, the silicone-fluid interface disappears at the submerged end of the tube and no distortion is observed in the background grid lines, while the tube is clearly visible above the liquid surface.

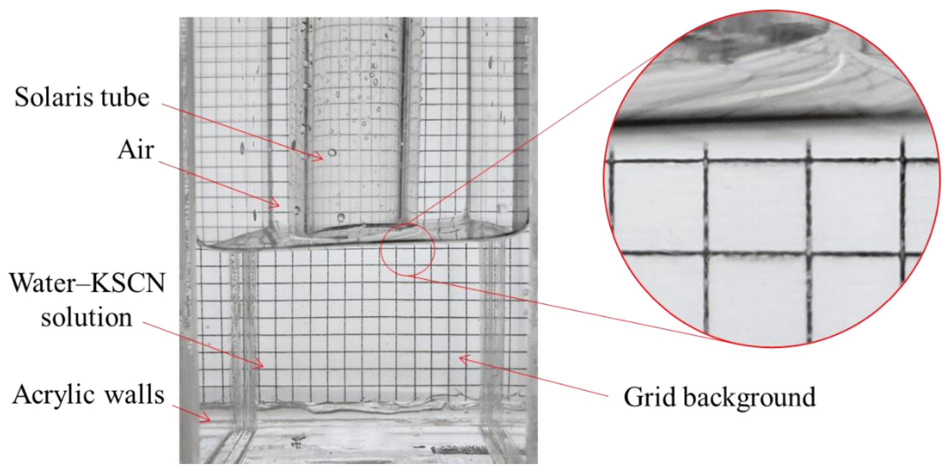

Fig. 4 Refractive index matching test. Solaris tube in water-KSCN solution.

As a first approach, time-resolved 2D3C PIV was applied to investigate the large-scale phenomena of a pulsatile flow within a compliant tube and the results of these experiments will be further used as a guide to interrogate smaller near-wall regions of interest in the flow. The measurements were performed using high-speed cameras (Phantom v611, Vision Research) with an 8-bit dynamic range, 1 megapixel resolution at a frame rate of 5 kHz and equipped with an 105 mm lens (AF Nikkor, Nikon Corporation). The field-of-view (FOV) was 27 × 17 mm, coincident with the axial cross-section of the tube and aligned at its mid-length, where its maximum expansion is expected. A calibration was performed by insertion of a dot target into the RIM fluid-filled chamber. The experiment was performed using a continuous-wavelength DPSS laser (LRS-0532 Series, Laserglow Technologies). The light sheet, which was approximately 1.5 mm thick, was formed with a pair of spherical and cylindrical lenses. A 2 μm diameter hollow glass spheres were the chosen tracer particles for this current phase of the study.

3. Results

Preliminary results were collected using a high-speed stereo imaging approach, with the diaphragm pump outputting a 36 mL stroke volume at a rate of 0.6 Hz. The camera frame rate was set to 5 kHz, and 8217 images were collected during each sampling of the flow field, equating to slightly less than one cycle at a time. The first frame of the camera was timed to coincide with the start of the compression stroke of the diaphragm pump using a function generator. Twelve cycles were captured in this way, processed using two-frame PIV in commercial software (DaVis 10.0.5, LaVision GmbH) down to a 32 × 32 window size with 50% overlap after algorithmic background removal and dynamic masking to isolate the fluid within the compliant tube. The results were then converted to mean axial velocity (y-direction) profiles by averaging the y-velocity in each image at each x-position. This results in the averaging of 27 the samples for each x-location on the profile, although these points are not spatially independent given they come from a single individual image pair. This produced velocity profiles for each of the 8217 time-points. Sample profiles are shown in Figure 5 for the primary flow acceleration during the pump compression stroke, near the peak of the flow rate, and during the primary deceleration phase.

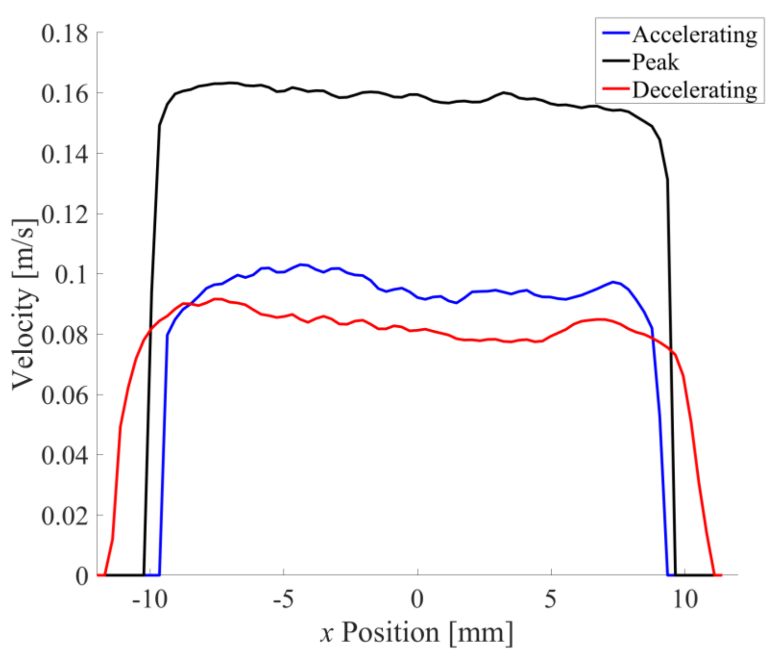

Fig. 5 Mean velocity profiles of flow acceleration during the pump stroke (blue), the peak flow during the cycle (black), and the deceleration phase (red).

Figure 5 shows that the profile during the accelerating and peak phase behaves as a "top-hat" profile, consistent with an accelerating or entry-region flow where the flow has not yet fully developed. An update to the flow system, adding a flow straightener before the test-section, has eliminated the previous asymmetry seen in the decelerating flow pictured in the preliminary abstract. Another point to note here is that the profile widens and thins in response to the expansion and contraction of the tube. The maximum tube diameter lags behind the peak flow rate, with the tube reaching maximum distension during the deceleration phase.

To present the data more completely, the profiles were combined into a surface in (x, t) space. This surface is displayed in Figure 6. The axial (y) velocity is displayed as both the height of the surface and in its coloration. Note that the blue border around the surface provides a strong visual reference point for 0 (zero) velocity. This shows the overall behavior of the flow over the complete cycle, with the flow first accelerating to a peak rate (Period 0.1-0.2), maintaining that peak rate briefly (Period 0.2-0.3), before decelerating (Period 0.3-0.4) and even reversing briefly (Period 0.45). This reversal is presumed to be due to a slow response-time in the closure of the valve. The flow then continues to slowly leak out of the tube as the tube returns to its initial diameter (Period 0.45+), with a second brief reversal (Period 0.68) thought to be a result of the oscillation of the tube's diameter. The change in tube diameter can be observed by looking at the border between the velocity profiles and the 0-velocity background as the PIV windows capture additional data along the edge of the expanding tube. An additional observation here is that there appears to be some oscillatory frequency superimposed over the overall flow; this will be discussed separately.

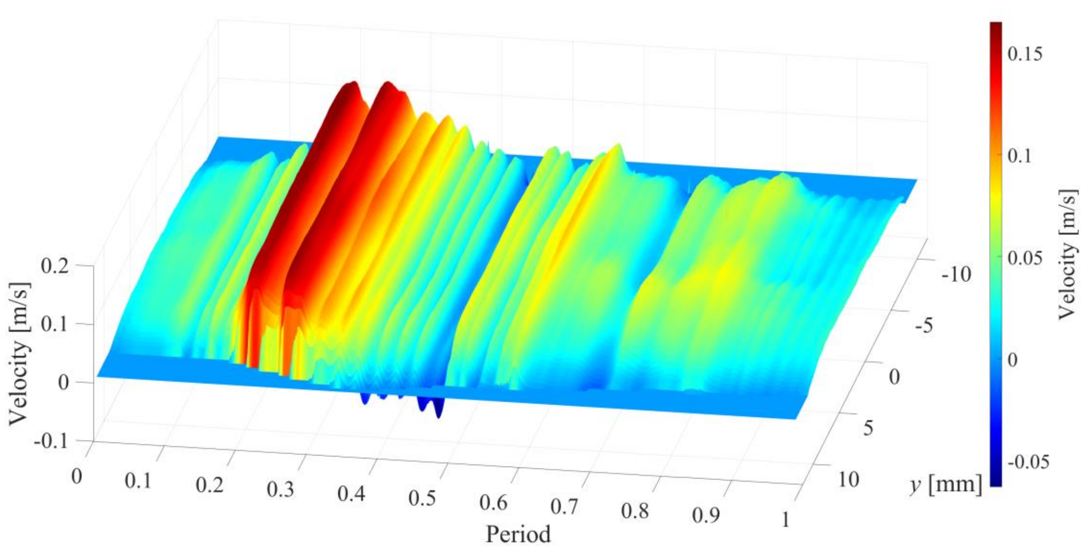

Fig. 6 Mean velocity profiles stacked in time to produce a contoured surface of y-velocity.

Displaying a side-view of the surface, in the (V, t) plane, provides insight into how the peak velocity varies as a function of time. This view is displayed alongside a measurement of the pressure just downstream of the tube, the tube width, and the pump's phase in Figure 7. The tube width was acquired by detecting the full-width half-maximum of the sum of intensity for each x-location in one of the stereo images. These plots provide insight into the interactions between the flow, pressure, and tube distension. The pump initially begins to accelerate around Period 0.1, producing the initial velocity peak (a). The pump continues, increasing the pressure of the system and the distension of the tube, before it begins to decelerate (b). As the pump decelerates, the flow decelerates as well, though it is still flowing into the tube at a faster rate than it is leaving. The tube reaches its maximum distension (c), peaking at the same time as the pressure in the system. As the pump begins its intake stroke, there is a lag time before the valve upstream of the measurement system closes, producing a brief flow reversal (d). Once the valve has closed, the forward flow resumes, driven by the tube's return to its initial diameter. The tube's natural frequency can be marginally observed in the tube width measurement, with secondary peaks after the maximal diameter at 0.35, spaced 0.25 of a period apart (e,g) indicating a natural frequency of around 2.4 Hz. A second brief flow reversal (f) may be related to this oscillation, but may also be due to a secondary opening of the upstream valve. These results are substantially different from those presented previously in the abstract, driven primarily by a flow restriction that was placed downstream of the measurement section. This restriction is responsible for slowing the outflow from the compliant tube, producing a pressure profile that is more reminiscent of the physiological pressure profile in the descending aorta (Alastruey at al., 2016) which the EVHP system seeks to replicate.

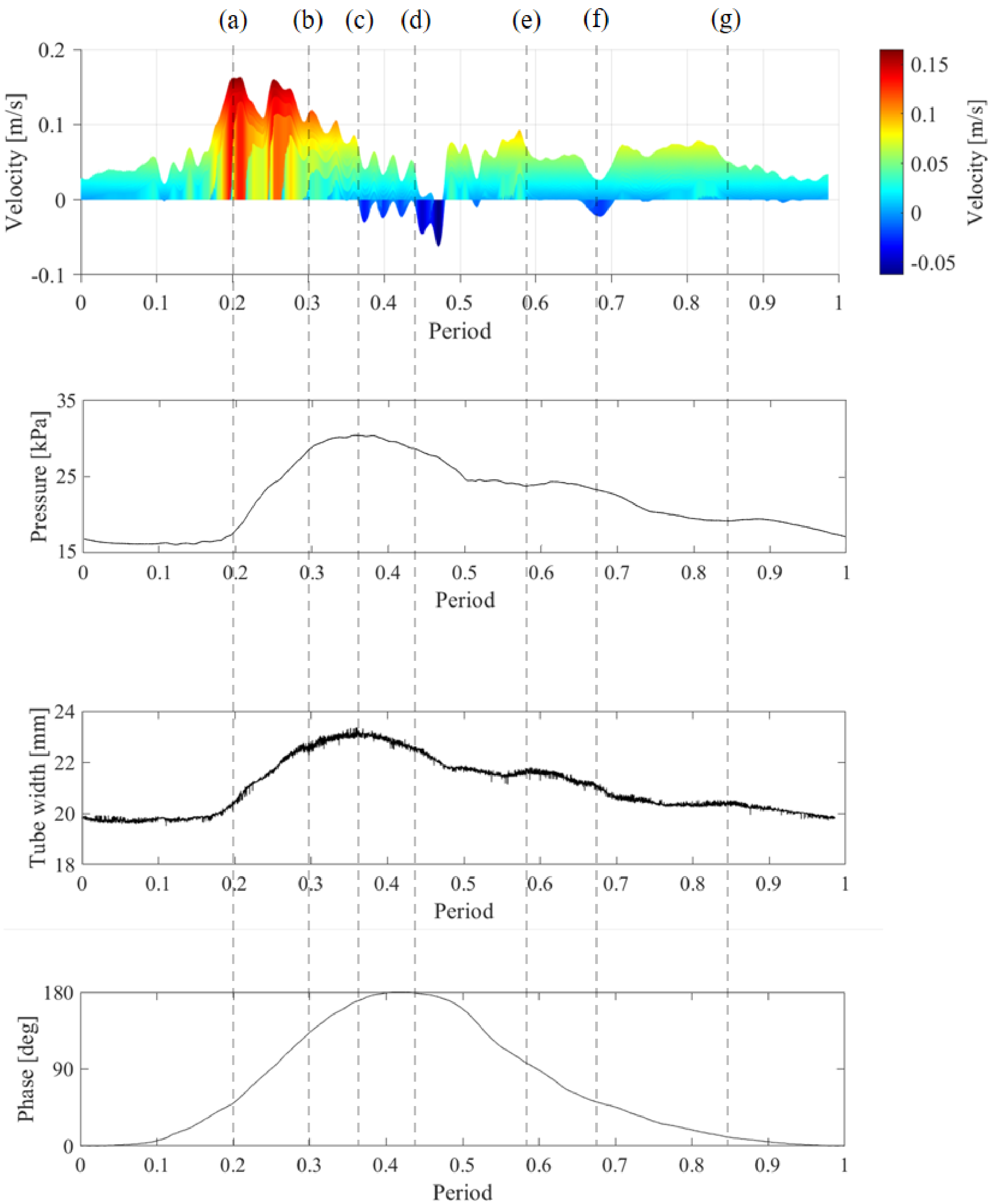

Fig. 7 Mean velocity profiles stacked in time (top) with the measured tube diameter (bottom). Vertical blue lines are used to denote key points in the relationship between the two curves.

In addition to the overall flow characteristics, these plots show a background, higher-frequency oscillation in the velocity field. In order to better observe this background frequency, three (V, t) profiles were extracted from the surface and these are plotted in Figure 8. These profiles indicate that the oscillation is relatively consistent across the width of the tube. There are several potential sources of this oscillatory mode. Given that the flow measurements shown are a mean profile over a 17 mm region, and that the amplitudes are similar regardless of the x-position, it seems likely that the oscillation is spatially independent, that is, it is likely occurring for the entirety of the observed flow simultaneously. It is hypothesized that the most likely reason for this oscillation is a non-linear response of the fluid-structure interaction between the pulsatile flow and the transient dynamic loading of the elastomeric tube wall. This highlights a need to further investigate the fluid domain close to the wall to understand the effect of compliance on the flow-pressure relationship and how compliance influences flow locally, in particular, the development of the viscous boundary layer. This phenomenon will be monitored in future experiments.

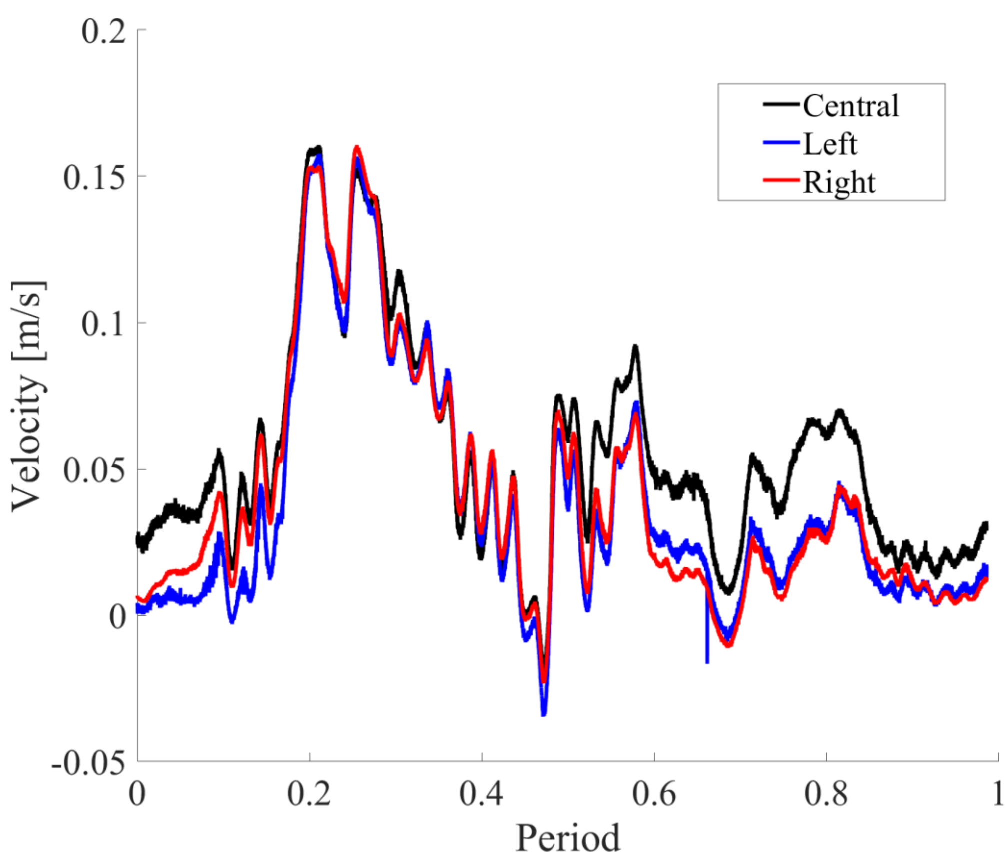

Fig. 8 Mean velocity in time of flow along the centre of the compliant tube, as well as two additional time-traces closer to the walls.

4. Conclusions

In addition to the general characteristics of a pulsatile flow through a compliant tube, the present study also reveals a potential complex fluid-structure relationship between the pulsatile flow and the moving tube wall characterized by a higher frequency background oscillation over the velocity field in the flow domain within the compliant tube. Experiments are being carried out to further investigate such phenomenon, this includes 2D3C time-resolved and turbulence intensity fields in the bulk flow of the compliant tube, in addition to the pressure waveforms at key points in the flow loop, improving upon the current results. These results will be used to find key locations in the flow's near-wall region upon which further investigations will be undertaken with stereo PIV to obtain 2D3C phase-averaged and turbulent intensity fields. The methodology for conducting the investigation and processing the data will follow the process from (Van Doorne & Westerweel, 2007), incorporating phase averaging techniques to allow measurement in the pulsatile flow. The results of this investigation will ultimately be used to improve the EVHP system.

Acknowledgements

The authors would like to acknowledge the support of the Natural Sciences and Engineering Research Council (NSERC) of Canada, the Canadian Foundation of Innovation (CFI), the Canadian National Transplant Research Program (CIHR/CNTRP) and the University Hospital Foundation (UHF).

References

Alastruey, J., Xiao, N., Fok, H., Schaeffter, T., & Figueroa, C. A. (2016). On the impact of modelling assumptions in multi-scale, subject-specific models of aortic haemodynamics. *Journal of The Royal Society Interface*, 13(119), 20160073.

Brindise, M. C., & Vlachos, P. P. (2018). Pulsatile pipe flow transition: Flow waveform effects. Physics of Fluids, 30(1), 015111.

Cameron, K., El Hassan, M., Sabbagh, R., Freed, D. H., & Nobes, D. S. (2020). Experimental investigation into the effect of compliance of a mock aorta on cardiac performance. PloS one, 15(10), e0239604. https://doi.org/10.1371/journal.pone.0239604.

Das, D., & Arakeri, J. H. (1998). Transition of unsteady velocity profiles with reverse flow. Journal of Fluid Mechanics, 374, 251-283.

Geoghegan, P.H., Buchmann, N.A., Spence, C.J.T., Moore, S., & Jeremy, M (2012). Fabrication of rigid and flexible refractive-index-matched flow phantoms for flow visualization and optical flow measurements. *Exp Fluids* 52, 1331–1347. https://doi.org/10.1007/s00348-011-1258-0.

Hino, M., Sawamoto, M., & Takasu, S. (1976). Experiments on transition to turbulence in an oscillatory pipe flow. Journal of Fluid Mechanics, 75(2), 193-207.

Konings, M. K., Jansen, R., Bosman, L. P., Rienks, R., Chamuleau, S. A., Rademakers, F. E., & Cramer, M. J. (2017). Non-invasive measurement of volume–time curves in patients with mitral regurgitation and in healthy volunteers, using a new operator-independent screening tool. Physiological measurement, 38(2), 241.

Ku, D. N. (1997). Blood Flow in Arteries. Annu. Rev. Fluid Mech. 29, 399–434.

Langlois, W. E., & Deville, M. O. (1964). Slow viscous flow (Vol. 173436). New York: Macmillan.

Lodahl, C. R., Sumer, B. M., & Fredsøe, J. (1998). Turbulent combined oscillatory flow and current in a pipe. Journal of Fluid Mechanics, 373, 313-348.

Van Doorne, C. W. H., & Westerweel, J. (2007). Measurement of laminar, transitional and turbulent pipe flow using stereoscopic-PIV. Experiments in Fluids, 42(2), 259-279.

White, C. W., Ambrose, E., Muller, A., Li, Y., Le, H., Hiebert, B., Arora, R., Lee, T. W., Dixon, I., Tian, G., Nagendran, J., Hryshko, L., & Freed, D. (2015). Assessment of donor heart viability during ex vivo heart perfusion. *Canadian Journal of Physiology and Pharmacology*. 93(10), 893-901. https://doi.org/10.1139/cjpp-2014-0474.

Womersley, J. R. (1955). Method for the calculation of velocity, rate of flow and viscous drag in arteries when the pressure gradient is known. The Journal of physiology, 127(3), 553–563. https://doi.org/10.1113/jphysiol.1955.sp005276.

Wood, N. B. (1999). Aspects of fluid dynamics applied to the larger arteries. J. Theor. Biol. 199(2), 137–161.